Probing the defect state of individual precipitates grown in an Al-Mg-Si alloy

Benedikt Klobes,* Björn Korff, Osman Balarisi, Patrick Eich, Matz Haaks, Karl Maier, and Reinhard Sottong
Helmholtz-Institut für Strahlen- und Kernphysik, Nußallee 14-16, D-53115 Bonn, Germany

Sven-Martin Hühne and Werner Mader
Institut für Anorganische Chemie, Römerstraße 164, D-53117 Bonn, Germany

Torsten E. M. Staab
Fraunhofer-Institut für Silicatforschung (ISC), Neunerplatz 2, D-97082 Würzburg, Germany
(Received 14 April 2010; revised manuscript received 7 July 2010; published 19 August 2010)

Precipitates forming in decomposable aluminum alloys such as Al-Mg-Si evolve toward the corresponding intermetallic phase, which is β (Mg_2Si) in this case, depending on heat-treatment conditions. Individual β precipitates were produced in an Al-1.11 at. % Mg-0.77 at. % Si alloy and identified using optical as well as electron microscopy. The individual β precipitates could be investigated with regard to their intrinsic crystal defects using a finely focused positron microbeam provided by the Bonn Positron Microprobe. Comparison with theoretical calculations of the Doppler broadening of annihilation radiation reveals that β precipitates most likely do not contain vacancies in either sublattice and that 0.16 is the upper bound of the fraction of trapped positrons. The usage of different enhancement factors had only little influence on the calculations whereas the general gradient approximation affected the contribution of Si orbitals, in particular. Additional measurements of the Doppler broadening based on the radioactive source ^{68}Ge, which emits high-energy positrons probing bulk regions of the sample, were carried out. These measurements show that β precipitates are sparsely distributed in the Al matrix.

DOI: 10.1103/PhysRevB.82.054113 PACS number(s): 78.70.Bj, 07.78.+s, 61.66.Dk, 81.30.Mh

I. INTRODUCTION

Ecological as well as economical considerations are driving forces for weight reduction in all areas related to transportation. Since weight saving results both in fuel efficiency and in protection of fossil fuels, great attention is drawn to the characterization and investigation of light-weight materials. For almost 100 years, aluminum-based alloys have been frequently applied in the automotive and aerospace industry because they combine high strength with light weight.[1] In particular, the interest in Al-Mg-Si-based alloys (the so-called AA6xxx series) has increased in recent years due to their high strength and their weldability. As in every age hardenable alloy, the favorable mechanical properties of Al-Mg-Si are induced by metastable clusters and precipitates which hinder dislocation movement. Usually, these structures are formed after solution heat treatment and quenching generating a supersaturated solid solution (SSSS) accompanied by a substantial concentration of quenched-in vacancies. During subsequent aging, the supersaturated solid solution is decomposed via vacancy-driven diffusion processes and the above-mentioned clusters and/or precipitates are formed. Depending on the exact alloy composition as well as on the parameters of the aging process (time and temperature) precipitates evolve according to a precipitation sequence which in the case of Al-Mg-Si can be summarized as follows:[2,3]

$$\text{SSSS} \rightarrow \text{clusters} \rightarrow \text{Guinier-Preston (GP) zones}$$
$$\rightarrow \beta''(\text{GPII}) \rightarrow \beta' \rightarrow \beta.$$

Initially, clusters containing the alloying elements are formed followed by plate such as GP zones which are fully coherent with the host matrix. Upon further aging, β'' precipitates (also referred to as GPII zones) evolve. Usually, the fully coherent β'' phase is supposed to cause the maximal mechanical strength of 6xxx alloys. Precipitation of β' and of the equilibrium phase β downgrades the mechanical properties of these alloys since both phases are coarsely dispersed and are at least partly incoherent with the Al matrix (see Ravi[3] for a detailed summary of the occurring phases).

Since the early 1980s positron annihilation spectroscopy (PAS) has been used as a unique tool to investigate the phenomenon of age hardening from a defect or vacancy-related perspective.[4] Conventional PAS techniques mainly utilize positrons emitted by radioactive isotopes, which usually probe bulk regions. In the course of the decay of ^{68}Ge, for example, positrons with an end-point energy of 1.89 MeV are emitted resulting in a mean penetration depth of 54 μm and a prolonged tail of hundreds of microns for aluminum. Thus, PAS studies using radioactive sources always average over a huge volume potentially containing only a small volume fraction of precipitates and defects. Spatial and lateral resolution in the micrometer range within the framework of PAS can only be achieved by means of positron microprobes which enable the focusing of slow positron beams.[5] Since the defect state of individual precipitates in Al alloys is an unexplored area up to now, it is the aim of this work to investigate embedded defects of β precipitates in Al-Mg-Si using the positron microbeam provided by the Bonn positron microprobe[6] (BPM). The interpretation of the positron annihilation data originating from individual precipitates is necessarily supported by theoretical calculations of the Doppler broadening of different possible annihilation sites. Measurements following the conventional radioactive source scheme for bulk investigations support the findings obtained by positron microscopy additionally.

II. EXPERIMENTAL DETAILS

A. Sample preparation

Two specimens with different dimensions were made from a laboratory Al-1.11 at. % Mg-0.77 at. % Si (Al-1.00 wt % Mg-0.80 wt % Si) alloy which was cast using high-purity base materials. This alloy thus contains silicon in excess above the stoichiometric composition of β (Mg_2Si). The thickness difference between the two samples (1 mm vs 3 mm) accounted for the different positron penetration depths $\bar{z}$ when using the 30 keV positron beam provided by the BPM or ^{68}Ge as a positron source [$\bar{z}$ (30 keV positron beam) $\approx$4.5 μm and $\bar{z}$ (99% of ^{68}Ge positrons) $\approx$2.5 mm, respectively]. Additionally, the thin sample was ground and polished down to 1 μm in order to enable optical as well as positron microscopy. Both samples were subjected to the same heat-treatment procedure which consisted of two steps. First the samples were solution heat treated for 2 h at 833 K and afterward aged at 623 K for 48 h in order to produce relatively coarse β precipitates. The complete heat treatment was conducted in high vacuum at approximately 1×10^{-6} mbar.

B. Experimental methods

Beside optical microscopy, scanning electron microscopy (SEM) combined with energy-dispersive x-ray (EDX) mapping was employed for surface investigations of the samples within this work. The defect state was probed by the spectroscopy of the Doppler broadening of annihilation radiation (DBAR) which is one branch of PAS. Positron annihilation techniques in general are characterized by their unique sensitivity to open-volume defects such as vacancies in which positrons are localized due to the missing core potential.[7,8] The Doppler broadening of the energy distribution of the annihilation quanta is thereby caused by the momentum distribution of electrons with which positrons annihilate since the momentum of thermalized positrons can usually be neglected. The longitudinal momentum component p_L of the annihilating electron along the direction of the annihilation γ ray results in an energy shift of $\Delta E=\pm\frac{p_L}{2m_0}$, where m_0 is the electron rest mass. The shape of the 511 keV annihilation line thus contains information about the electron momentum distribution at the annihilation site. While the central part of the annihilation line contains information about the open volume of the annihilation site, its wings, i.e., the high momentum region $p_L\geq10\times10^{-3}m_0c$, carry information about the chemical species of the next-neighboring atoms. Comparing experimental data with suitable references or models it is therefore possible to determine the annihilation site and its chemical surroundings in some cases.

For bulk DBAR measurements, samples have been placed in a vacuum chamber with a positron source placed directly on top of them in order to avoid the usual sandwich geometry which requires two identical samples.[9] The annihilation radiation is then detected using a high-purity germanium detector with an energy resolution of about 1.35 keV at 478 keV. The 478 keV line of ^{7}Be is used supplementary to stabilize the measurement electronics. For spatially resolved DBAR investigations, the BPM is employed. Its monoenergetic positron beam of 30 keV exhibits a mean penetration depth of about 3.4 μm in aluminum. Properties of the positron microbeam as focus position or beam diameter can be adjusted by magnetic lenses according to the experimental requirements.[6] Since the positron beam guidance is right angled due to a magnetic prism, the detector can be effectively shielded from any disturbing high-energy background radiation emitted by the ^{22}Na source itself or caused by annihilation events in the horizontal part of the BPM.[6] At the same time, all positrons passing through the magnetic prism can be directed onto the sample reliably. Any background at 511 keV is thus only caused by positrons backscattered from the sample. Since the BPM is equipped with a SEM, samples can be oriented and mapped in an easy way.[6] As in the conventional DBAR case, the annihilation quanta are detected with a high-purity Ge detector featuring an energy resolution of 1.25 keV at 478 keV.

Using a single germanium detector usually limits the resolvable momentum range to $p_L\leq10\times10^{-3}m_0c$ due to the relatively low signal to background ratio up to 1/1000 for $p_L\geq10\times10^{-3}m_0c$. Nevertheless, it is possible to overcome this limitation by means of the high momentum analysis (HMA) method. This approach entails a sophisticated procedure of background determination and subtraction. The only prerequisite is the absence of γ background above the annihilation peak at 511 keV. In the case of slow positron beams, such as the BPM, this can be achieved by an appropriate shielding of the germanium detector as discussed above. For conventional DBAR measurements employing radioactive sources, a positron emitter with negligible low-γ background as ^{68}Ge has to be used. The details of the HMA method and its applicability are described by Haaks.[10]

Results of the high momentum region of DBAR measurements can be easily elaborated by ratio plots, which are obtained by normalizing spectra under investigation on a reference DBAR curve. Figure 1 exemplarily shows the ratio plots of pure Mg, Si, and Cu with respect to annealed Al. Differences in the electron momentum distribution probed by positrons are clearly reflected in the shape of the ratio plots. Probing Al alloys containing few percents of alloying atoms these shapes can be used to identify the chemical environment of the positron annihilation site. Moreover, the combination of the spatial resolution facilitated by the BPM with the HMA method allows for a spatially resolved chemical analysis of crystal defects in materials using positrons.

III. THEORETICAL METHODS

Especially in the high momentum region, the interpretation of experimental DBAR data often presupposes standards for comparison. If these standards cannot be obtained or if measurements of standards themselves are to be interpreted, one has to resort to theoretical calculations. In this work, numerical calculations of the Doppler broadening of annihilation radiation were performed employing the program DOPPLER.[11,12] In this approach, the electron density is constructed by a superposition of atomic orbitals. The positron wave function is calculated in a 96 atoms supercell on a

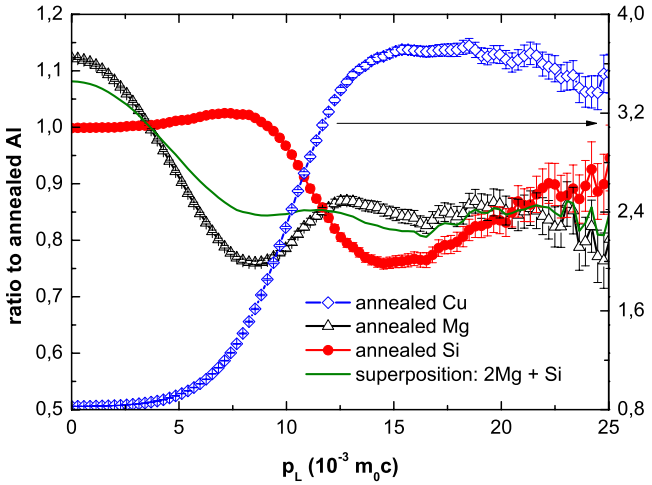

FIG. 1. (Color online) Ratio plots of Mg, Si (left ordinate), and Cu (right ordinate) with respect to annealed Al. Differences in positron localization and electron momentum distribution produce a characteristic fingerprint curve which can aid the analysis of compound or alloy ratio plots containing Mg, Si, and/or Cu. Additionally, an elemental superposition of Mg and Si in the stoichiometrical composition of β is shown.

64^3-mesh real-space grid using potentials derived by density-functional theory (DFT) methods.[13] From the overlap of electron and positron densities, the annihilation rate for each orbital is calculated. The increase in the annihilation rate due to the attraction of electrons by a positron can be described by different enhancement factors,[14,15] which can be employed either in the local-density approximation (LDA) or the general gradient approximation (GGA) for the exchange-correlation energy.[12] The electron momentum distribution probed by positrons is then obtained by summing up each electron state weighted by the calculated partial annihilation ratio. Since this procedure is based on electron wave functions of free atoms, bonding effects on the valence-electron density are neglected, which leads to an artifact in the low momentum region of positron annihilation, due to the poor description of valence electrons. Nevertheless, the high momentum region $p_L \geq 10 \times 10^{-3} m_0 c$ is usually well modeled by this approach because there mainly electrons with high momenta, i.e., core electrons not taking part in the bonding process, contribute to the annihilation process. Since the chosen enhancement factor and its combination with LDA or GGA may have an impact on the calculated DBAR, all calculations were performed within LDA as well as GGA using the cited enhancement factors. The calculated DBAR curves were additionally convolved with a Gaussian function of appropriate width (1.25 keV) in order to ascertain comparability with experiment.

Previous to the calculation of the DBAR spectra the corresponding structures, which partially contain vacancies (cf. Sec. V), were relaxed using the *ab initio* code SIESTA,[16] i.e., the atomic coordinates in presence of a vacancy were recalculated. SIESTA is a density-functional theory code in the local-density approximation which utilizes a local Gaussian basis set within the split-valence method.[17] The Brillouin zone is thereby sampled by a Monkhorst-Pack mesh. The relaxations of β-based structures were carried out with supercells of 96 atoms and a double-zeta basis set plus polarization orbitals. The meshs in k and real space consisted of 3^3 and 72^3 points, respectively. More details as well as the results of this relaxation procedure are described by Staab.[18]

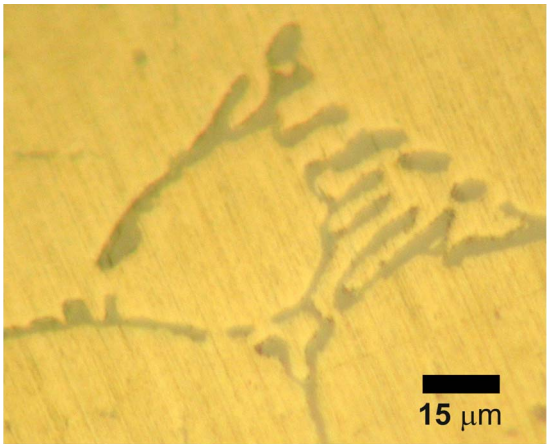

FIG. 2. (Color online) Optical bright-field micrograph of β precipitates. The β phase usually precipitates in a complex morphology which is also referred to as *chinese script* and appears bluish.

IV. EXPERIMENTAL PROCEDURE

Using the thick sample bulk properties were probed by a DBAR spectrum obtained with a ^{68}Ge positron source having an activity of about 0.3 MBq. The annihilation radiation thus stems from a volume of several cubic millimeter averaging over precipitates and aluminum matrix as well.

The first step toward the investigation of an individual β precipitate by means of the BPM was the identification of single precipitates at the surface of the thin sample. This was achieved using both optical and electron microscopy. Since the β phase is known to appear bluish in optical bright-field microscopy and to exhibit a *chinese script* morphology,[19] potential precipitates were initially identified this way. Figure 2 displays an example of the complex morphology of the β precipitates.

In order to verify potential β precipitates for further investigations and to estimate their extension below the surface, the precipitates were additionally imaged using an electron microscope JEOL JSM-6400F operated at 25 kV and equipped with an EDX mapping system including a HPGe detector. Exemplarily, EDX maps of a single β precipitate are shown in Fig. 3. Although the exact stoichiometry of β is hardly determinable using EDX analysis due to the low atomic number of Mg and Si, the obtained EDX maps clearly indicate the absence of Al inside the precipitates [cf. Fig. 3(a)]. Assuming that the mean penetration depth of 25 keV electrons approximates the value for 30 keV positrons, the absence of an Al signal shows that the depth extension of these precipitates is sufficient to stop the vast majority of positrons provided by the BPM. Furthermore, in combination with the optical appearance of the precipitates the EDX mapping results thus show that the precipitates correspond to the β phase in fact.

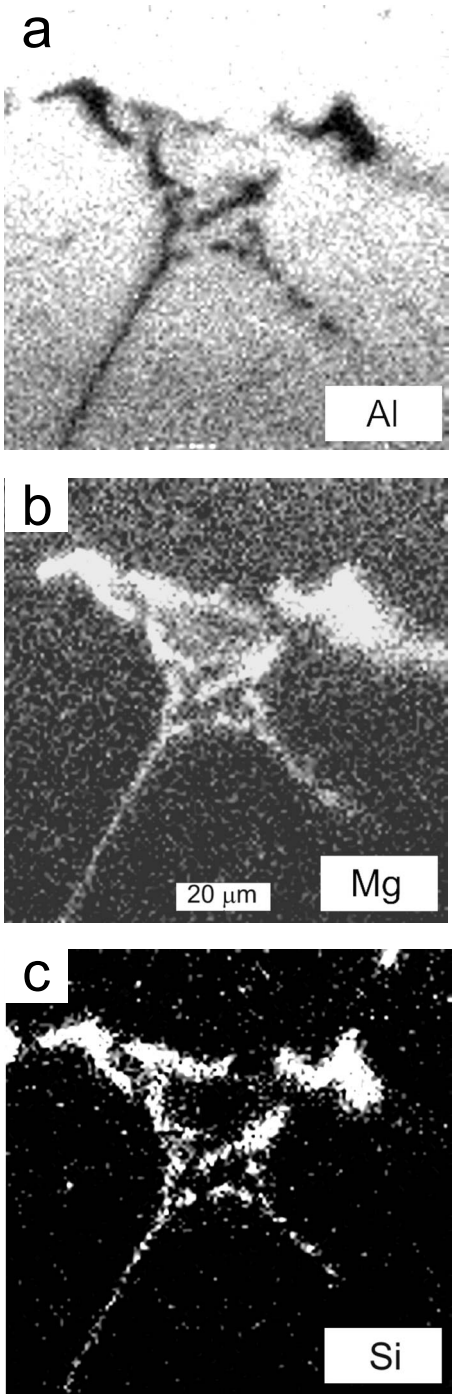

FIG. 3. Element-specific EDX maps of an individual β precipitate. Bright points indicate the presence of the specific element at the particular site.

Once a precipitate position had been determined by the SEM facility of the BPM and the beam dimensions had been reduced below the actual precipitate size, the corresponding β phase precipitate as well as a precipitate free area (the matrix) were measured with the fine focus positron microbeam. The precipitates usually had an expanse with a diameter of at least 10 μm, onto which the beam diameter (usually about 8 μm) could be easily scaled. Reference

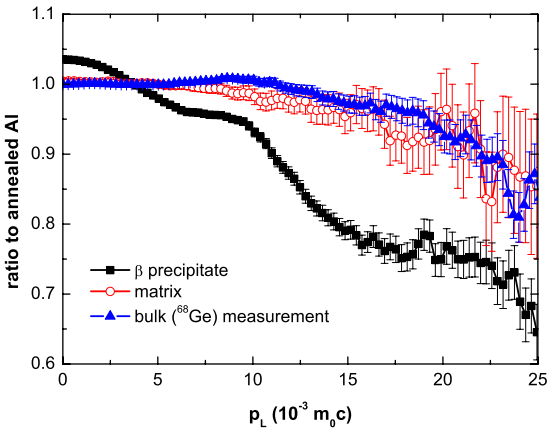

FIG. 4. (Color online) Ratio plots of an individual β phase and matrix measurements using the BPM. No influence of vacancies and only weak indications of alloying elements can be detected in the matrix. By contrast, focusing the positron beam onto an individual precipitate yields a significant decrease in the high momentum region and an increase in the low momentum region.

measurements of an annealed Al sample were performed right after that.

V. RESULTS

The DBAR ratio plots of an individual β precipitate and the corresponding alloy matrix measurement obtained using the fine focus microbeam of the BPM are shown in Fig. 4. The matrix measurement does not indicate any significant contribution of positron annihilation in vacancylike defects or precipitates. Since merely in the high momentum region its ratio plot deviates from the pure Al ratio, which would be a constant value of one, the matrix measurement reflects positron annihilation in bulk Al containing only a minimal contribution of alloying atoms or possibly small Si clusters. In contrast to this, an individual β-type precipitate yields a characteristic ratio plot both in the low and in the high momentum region. Thus, using a fine focus positron beam, the decomposition and accordingly the precipitation process in Al alloys can be probed on a micron scale. Comparing the precipitate signal to the one obtained employing the conventional DBAR scheme averaging over the volume (cf. Fig. 4) reveals that positron annihilation in β precipitates is rather insignificant and that the spectrum is dominated by annihilation events in the Al matrix. The β precipitates are sparsely distributed in the Al matrix and thus neither the precipitates themselves nor the associated phase boundaries trap a significant amount of positrons in the course of bulk measurements. The small difference between the alloy matrix measurement using the positron microbeam and the bulk measurement using the radioactive source arises mainly from the different volumes, which are probed by these two approaches, and from a minimal capture of positrons in β precipitates in the case of the bulk measurement. Moreover, the comparison of the DBAR of an individual precipitate with the stoichiometric superposition of annealed Mg and Si as shown in Fig. 1 shows that the electron momentum distribu-

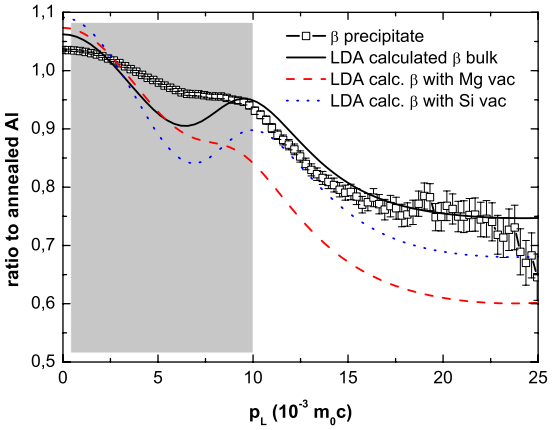

FIG. 5. (Color online) Comparison of theoretical ratio plots of different possible annihilation sites in β using the local-density approximation with the experimental curve. The sphere of systematic calculational deviations is shaded in gray.

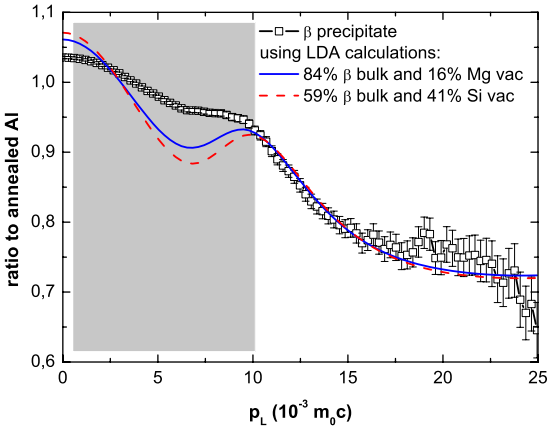

FIG. 6. (Color online) Linear combination of calculated β bulk DBAR with the Si or Mg vacancy signal using LDA. The assumption of a superposition of annihilation in bulk β and annihilation in vacancies can be used to minimize the deviation from the experiment in the high momentum region. Both assumptions agree with the experimental data.

tion in β cannot be understood as a superposition of its constituents.

Since the individual β precipitate ratio plot exhibits an increase in the low momentum region compared to annealed Al, one might be apt to attribute this feature to open-volume defects, which is a common interpretation of similar DBAR data concerning Al alloys. However, since the annihilation radiation definitely stems from the inside of the investigated β precipitate, theoretical calculations of the DBAR spectra of possible annihilation sites exclusively allow for a consistent interpretation of the experimental data. Therefore, DBAR calculations of positron annihilation in the bulk β crystal, in a Mg vacancy of β and in a Si vacancy of β were performed according to the explanation given in Sec. III.

The usage of different enhancement factors within LDA or GGA had only little influence on the calculated Doppler broadening. Moreover, the changes due to enhancement factors are rather independent from the underlying structures. Therefore, using ratio plots different enhancement factors yield the same results. In the following, the calculations are thus identified by the labels LDA or GGA without reference to the enhancement factor used.

In the first instance, the calculations on the basis of LDA are displayed in Fig. 5 and show that an increase in the low momentum region is to be expected in any case. Though the low momentum region of the calculations suffers from systematic errors (cf. Sec. III), the high momentum region can be used to interpret the experimental data. Since the experimental curve runs below the calculated β bulk DBAR ratio plot but above the theoretical curves of both types of vacancies, positron trapping in this case has to be regarded as incomplete, i.e., a considerable fraction of positrons annihilates in bulk β regions without being trapped in vacancies. Moreover, it is possible to model the experimental result as a superposition of the calculations by introducing the fraction of trapped positrons η. Assuming a linear combination of annihilation events in β bulk and in one type of vacancy, i.e., either annihilation in a vacancy in the Mg sublattice or in the Si sublattice, the error-weighted square deviation in the high momentum region can be minimized by 16% or by 41%, respectively. These results are shown in Fig. 6. The possibility of both Si and Mg vacancies is not taken into account since several fractional combinations are possible to reproduce the experimental data. Furthermore, the fact that the alloy contains Si in excess rather supports the assumption of Mg vacancies. In either case (with respect to the LDA calculations), annihilation in bulk β dominates, although in the case of Si vacancies its fraction is reduced to about 59%, which thus represents the minimum contribution of annihilation in bulk β.

The calculations using GGA are shown in Fig. 7. In comparison with the LDA calculations shown in Fig. 5 employing the GGA mainly results in a slight vertical shift of the ratio plots. In this case, the experimental β ratio plot fits the calculated β bulk one very well, i.e., there is no indication of positron trapping into vacancies employing GGA calculations. Comparing LDA with GGA calculations of the same atomic structure, the influence of the general gradient approximation seems to be stronger if there is Si at the annihilation site. While the overall change due to GGA is relatively

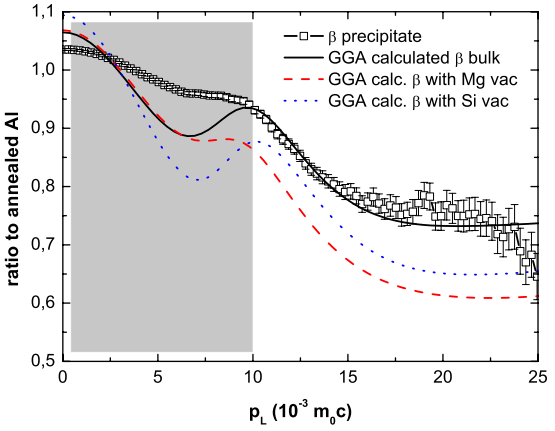

FIG. 7. (Color online) Comparison of GGA calculations of different possible annihilation sites in β with the experimental one.

low in the case of the vacancy on the Si sublattice, its impact on bulk β as well as on the vacancy on the Mg sublattice is more pronounced. Finally, it should also be noted that both LDA and GGA calculations reproduce the general trend of the β ratio plot even in the low momentum region though the amplitude is significantly overestimated.

VI. DISCUSSION

From a methodological point of view, the presented measurements and calculations imply two main findings. On the one hand, the HMA proves to be a valuable tool accessing the high momentum region of DBAR spectra not only in the case of annealed pure metals. It represents thus an alternative to the well-established coincidence Doppler broadening spectroscopy[20] employing two Ge detectors for background rejection. This is especially true for all cases in which a configuration of two detectors is impossible for geometrical or other reasons. On the other hand, the experimental data could be uniquely interpreted using theoretical calculations since experimental standards for β precipitates are not accessible. Combining these calculations with PAS thus allows for employing PAS for the chemical analysis of defect complexes in materials.

Concerning the precipitation of β in the Al-Mg-Si alloy, the spatially resolved DBAR measurements clearly show a distinct differentiation between β precipitates and precipitate-free regions, i.e., the matrix. The matrix measurement greatly resembles the DBAR spectrum obtained using the radioactive positron source, which averages over a huge volume. Therefore, without using a focused positron beam there is only little positron trapping in β precipitates since they are sparsely distributed in the Al alloy matrix.

Calculations of different possible annihilation sites in β were carried out using different enhancement factors within LDA as well as GGA. The choice of a particular enhancement factor had a rather small influence on the calculations, which can surely be ascribed to the relative similarity of the electronic structure of Mg, Al, and Si. Employing GGA the contribution of the high momentum core electrons is decreased resulting in a lowering of the corresponding ratio plots. Since this applies for calculations of bulk β and a vacancy on the Mg sublattice but not for a vacancy on the Si sublattice, the decrease in the high momentum region can be attributed to a change in partial annihilation rates of Si orbitals. Furthermore, the vacancy concentration inside β precipitates is rather small, which could be proven by the discussed theoretical DBAR calculations. Based on LDA calculations, the fraction of positrons trapped in Mg vacancies can be estimated to be about 16%. Although the comparison between calculation and experiment does not allow for distinguishing between Mg or Si vacancies the former is most likely since the investigated alloy contains Si in excess above the stoichiometric composition of β. However, the GGA calculations suggest that β precipitates do not contain any defects within the dynamic range of positron annihilation spectroscopy. In any case, the systematic error of the estimated fraction of trapped positron strongly depends on the accuracy of the DBAR calculations. This is ensured by the restriction of the fit procedure on the momentum range $10\times10^{-3}m_0c \leq p_L \leq 25\times10^{-3}m_0c$, in which mainly core electrons not affected by bonding effects contribute. In addition, the qualitative similarity between the experimental results and all the calculations performed indicate that the core electrons are not affected by the Mg-Si interaction in β. Nevertheless, an accurate and direct determination of the fraction of trapped positrons in this case requires a Positron Lifetime Spectrometer with spatial resolution in the micron range, which unfortunately is not operational.

VII. CONCLUSIONS

In this work, we have shown that the defect state of individual precipitates grown in Al-Mg-Si alloys can be uniquely investigated using positron microscopy. Precipitates of the equilibrium phase β were initially identified using optical and electron microscopy including EDX mapping. Spatially resolved measurements of individual β precipitates and matrix regions reveal great differences between the corresponding DBAR data. Additional measurements following the conventional DBAR method, which utilizes radioactive positron sources, show that the defect state of individual precipitates can be uniquely accessed with positron microbeams.

Theoretical DBAR calculations of different possible annihilation sites in β precipitates, namely, bulk β or Mg and Si vacancies in β, respectively, were carried out employing different calculational schemes, i.e., different enhancement factors in combination with LDA or GGA, respectively. While the calculations are rather independent of the enhancement factor, there are significant differences between GGA and LDA. The present findings suggest that these are mainly sensitive to Si orbitals. Using these calculations, it could be deduced that positron annihilation in β precipitates is dominated by annihilation in the bulk β crystal. GGA calculations indicate that β precipitates grow without incorporation of vacancies. In this context, the usual correlation of an increased low momentum region with a vacancy concentration could be shown to be erroneous in this case.

Furthermore, the procedure presented in this work should be applicable to all systems containing separate phases embedded in matrix. This is especially true for decomposable Al alloys forming precipitates of adequate size, e.g., other important classes as Al-Cu- or Al-Zn-based alloys.

ACKNOWLEDGMENTS

Parts of this work have been financially supported by the Deutsche Forschungsgemeinschaft (Grant No. STA 527/3-2). We would also like to thank John Banhart for useful comments on the manuscript.

*klobes@hiskp.uni-bonn.de

[1] E. Hornbogen, J. Light Met. **1**, 127 (2001).
[2] I. Dutta and S. Allem, J. Mater. Sci. Lett. **10**, 323 (1991).
[3] C. Ravi and C. Wolverton, Acta Mater. **52**, 4213 (2004).
[4] A. Dupasquier, G. Kögel, and A. Somoza, Acta Mater. **52**, 4707 (2004).
[5] O. Toshitaka, J. Satoshi, and F. Masanori, Anal. Sci. **25**, 837 (2009).
[6] H. Greif, M. Haaks, U. Holzwarth, U. Männig, M. Tongbhoyai, and K. Maier, Mater. Sci. Forum **255-257**, 641 (1997).
[7] M. Puska and R. Nieminen, Rev. Mod. Phys. **66**, 841 (1994).
[8] P. Schultz and K. Lynn, Rev. Mod. Phys. **60**, 701 (1988).
[9] K. Bennewitz, M. Haaks, T. Staab, S. Eisenberg, T. Lampe, and K. Maier, Z. Metallkd. **93**, 778 (2002).
[10] M. Haaks, T. Staab, and K. Maier, Nucl. Instrum. Methods Phys. Res. A **569**, 829 (2006).
[11] M. Alatalo, H. Kauppinen, K. Saarinen, M. J. Puska, J. Mäkinen, P. Hautojärvi, and R. M. Nieminen, Phys. Rev. B **51**, 4176 (1995).
[12] M. Alatalo, B. Barbiellini, M. Hakala, H. Kauppinen, T. Korhonen, M. J. Puska, K. Saarinen, P. Hautojärvi, and R. M. Nieminen, Phys. Rev. B **54**, 2397 (1996).
[13] M. Puska and R. Nieminen, J. Phys. F: Met. Phys. **13**, 333 (1983).
[14] E. Boroński and R. M. Nieminen, Phys. Rev. B **34**, 3820 (1986).
[15] B. Barbiellini, M. J. Puska, T. Torsti, and R. M. Nieminen, Phys. Rev. B **51**, 7341 (1995).
[16] J. Soler, E. Artacho, J. Gale, A. Garcia, J. Junquera, P. Ordejón, and D. Sánchez-Portal, J. Phys.: Condens. Matter **14**, 2745 (2002).
[17] J. Junquera, Ó. Paz, D. Sánchez-Portal, and E. Artacho, Phys. Rev. B **64**, 235111 (2001).
[18] T. E. M. Staab, Phys. Status Solidi B **246**, 1587 (2009).
[19] *ASM Handbook*, edited by K. Mills (ASM International, Materials Park, Ohio, 2000), Vol. 9.
[20] K. Lynn, J. MacDonald, R. Boie, L. Feldman, J. Gabbe, M. Robbins, E. Bonderup, and J. Golovchenko, Phys. Rev. Lett. **38**, 241 (1977).